Korean J. Chem. Eng., 38(4), 797-806 (2021)
DOI: 10.1007/s11814-021-0753-0

pISSN: 0256-1115
eISSN: 1975-7220

Hydrothermal carbonization of oil palm trunk via taguchi method

Sundus Saeed Qureshi*, Premchand, Mahnoor Javed***, Sumbul Saeed****,†, Rashid Abro**, Shaukat Ali Mazari**, Nabisab Mujawar Mubarak*****,†, Muhamad Tahir Hussain Siddiqui******, Humair Ahmed Baloch******, and Sabzoi Nizamuddin******,†**

*Institute of Environmental Engineering and Management, Mehran University of Engineering and Technology, Jamshoro 76090, Sindh, Pakistan
**Department of Chemical Engineering, Dawood University of Engineering and Technology, Karachi 74800, Sindh, Pakistan
***Institute of Chemistry, University of Punjab, Lahore-54590 Punjab, Pakistan
****College of Plant Sciences and Technology, Huazhong Agricultural University, Wuhan 430070, P. R. China
*****Department of Chemical Engineering, Faculty of Engineering and Science, Curtin University, 98009 Sarawak, Malaysia
******School of Engineering, RMIT University, Melbourne 3000, Australia
(*Received 26 November 2020 • Revised 20 January 2021 • Accepted 26 January 2021*)

Abstract−Hydrothermal carbonization (HTC) and its parameters show a significant role in the quality of HTC products and the distribution of yield. The present study investigates the optimal conditions that are suitable to produce maximum yield products of solid, liquid, and gas, from HTC of oil palm trunk (OPT), by following the Taguchi method. Moreover, all the three products of HTC were analyzed using various characterizations. The optimum runs for hydrochar yield, liquid yield, and gaseous yield were run 1 (R1), run 4 (R4), and run 9 (R9), respectively. The reaction temperature was found to be the most influential parameter that affected the yield distribution during HTC, where low temperature supported solid production, intermediate temperatures favored liquid yield, and high temperature produced higher gaseous yield. Elemental analysis, H/C and O/C atomic ratios, higher heating value (HHV), and energy density values of hydrochar recommended that the HTC process has significantly converted OPT into better energy fuel. The energy densification value of hydrochar ranged between 1.28 and 1.40, which confirmed the significance of the HTC process. Two characteristic peaks from FTIR were observed at 3,430 cm^{-1} and 2,923 cm^{-1} hydrochar. SEM analysis confirmed that the porosity of hydrochar was higher than OPT after HTC. However, the major organic matter in the bio-oil traced by GC-MS analysis was acetic acid, accounting for about 59.9-71.7%, and the outlet gaseous product consisted of 0.87-9.17% CH_4, 3.88-29.02% CO_2, 1.07-7.89% CO, and 0.31-1.97% H_2, respectively, as shown by GC-TCD.

Keywords: Hydrothermal Carbonization, Oil Palm Trunk, Taguchi Method, Analysis of Variance

INTRODUCTION

Biomass is one of the most widely used organic materials that can be converted into three distinct forms of bioenergy fuels, such as solid, gaseous, and liquid [1-3]. Among these, solid fuel has tremendous characteristics to come through future energy resource due to outstanding features, such as greater thermal, chemical, structural properties, and better energy values. Solid fuel is primarily known as biochar, produced from pyrolysis of biomass [4,5], and hydrochar produced by hydrothermal carbonization (HTC) of biomass [6,7]. HTC is an eco-friendly technique that is carried out at 180-250 °C and 2-10 MPa in the presence of water for several hours, whereas water itself acts as a solvent as well as reactant [8]. In the HTC process, water itself contributes to the increase in the process of carbonization of biomass by modifying the yield distribution to solid, liquid, and gaseous fuels. Furthermore, the distribution of the product of HTC relatively depends on different factors such as reaction temperature, particle size, reaction time, feedstock, reaction environment, as well as heating system (conventional or microwave) [9]. Consequently, we strongly analyzed the effect of reaction time, reaction temperature, and particle size on the distribution of the yield of HTC of oil palm trunk (OPT) to solid, gaseous, and

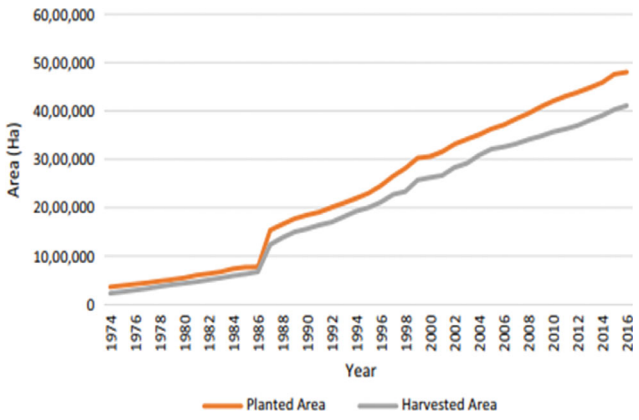

Fig. 1. Area of oil palm plantation in Malaysia from 1972 to 2016 [14].

†To whom correspondence should be addressed.
E-mail: sumbulsaeed717@gmail.com, mubarak.mujawar@curtin.edu.my, mubarak.yaseen@gmail.com, nizamuddin248@gmail.com

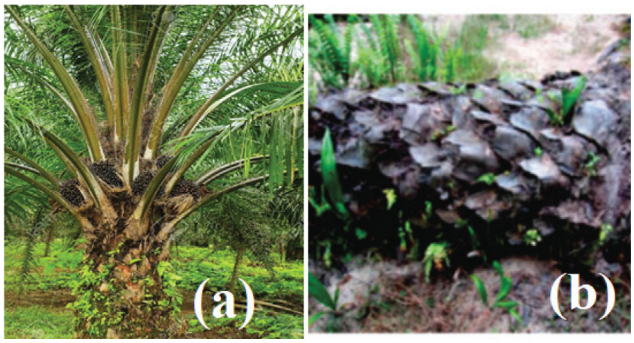

Fig. 2. (a) Oil palm tree and (b) OPT.

liquid yields, respectively.

The oil palm tree is the largest produced plant in Malaysia, where the total planted and harvested area of oil palm in Malaysia is shown in Fig. 1. The OPT is a major constituent of oil palm tree produced at plantation sites [10] after every 25-30 years during the replanting season of oil palm trees [11], and mainly contains 70% of total source by weight [12]. Fig. 2(a) shows the oil palm tree and Fig. 2(b) displays OPT. The composition of lignocellulose for OPT contains 34.4% cellulose, 23.9% hemicellulose, and 35.9% lignin, and the elemental composition of OPT consists of 5.6% hydrogen, 42.7% carbon, 51.2% oxygen, and 0.44% nitrogen, whereas proximate analysis of OPT contains 5.3% ash, 82.6% volatile matters, 7.2% moisture contents, and 4.9% fixed carbon, respectively [12]. Because of the logistics and storage issues, less attention has been focused to OPT, though it has been greatly and efficiently utilized as a renewable energy resource by modifying itself into other forms of energy such as biofuels [11,13]. Sustainably, it is assumed that the conversion of biomass into other forms of energy is much more effective and useful rather than direct burning biomass. Because, direct burning will produce a huge amount of pollutants that are hazardous for human health and the environment. One promising technique to handle large amounts of biomass wastes including OPT is to convert OPT into liquid (bio-oil), solid (hydrochar), and gaseous (biogas) through HTC process. The main product of HTC is hydrochar, while biogas and bio-oil are by-products of HTC process.

Hydrochar is a carbonaceous component with exceptional physicochemical properties, such as an increase in the heating rate and decrease in fibrous structure formed by the thermal degradation of biomass or its derivatives, having application in the process of water purification, catalysis, soil amendment, and gas storage [15]. Hydrochar formed from various biomass sources has been greatly employed for many applications, such as carbon catalysts to form chemicals, carbon material for increasing the fuel cells efficiency, carbon nanomaterials, solid fuel, soil fertility process, capacitor, energy production, and adsorbent for carbon dioxide sorption water purification process [16]. Because of the porous geometrical structure and functionalized/aromatic/reactive surfaces [17], hydrochar is chiefly well-known as an efficient adsorbent for eliminating contaminants from water. Many researchers have articulated that hydrocar is a suitable adsorbent for removing lead (Pb) [6,18], cadmium (Cd) [7], phosphorous [19], methylene blue [6], and malachite green. Hammud et al. [20] examined and compared the sorption capability of biochar and hydrochar for the removal of organic contaminants.

The main objective of the present study was to use undervalued biomass obtained from the oil palm industry, i.e., OPT through the HTC process. The effects of the HTC process and its parameters have been optimized for the yield of solid, liquid, and gaseous via the Taguchi method. Additionally, hydrochar and bio-oil have been primarily well-characterized for fuel applications to evaluate the efficacy of bio-oil as a liquid fuel and hydrochar as a solid fuel.

MATERIALS AND METHODS

1. Collection of OPT Material

The OPT was collected from oil palm plantations in FELCRA Nasiruddin, Bota, Perak, Malaysia. Initially, OPT was washed with distilled water to remove impurities and dirt, further dried in an oven at 105 °C, and finally, ground to 1-3 mm particle size with the help of IMF 10 basic, IKA Labortechnik crusher. The OPT was characterized for elemental analysis, proximate analysis, and HHV as shown in Table 1.

2. Experimental Procedure for HTC of OPT

The HTC of OPT was carried out in a high-pressure stainless-steel autoclave reactor with a volumetric capacity of 1,000 mL as shown in Fig. 3, where 20 mg of OPT was mixed with distilled water at the ratio of 1 : 10 (w/v). Initially, nitrogen gas was purged at 3 bar for 5 min to confirm that the reactor is tightly fixed and there was no space for leakage, after that the reactor was purged with 10 bar nitrogen (99.9% pure) to avoid any vaporization, and to preserve the liquid phase at high temperature and high pressure of the HTC process. The reaction was carried out at the suggested reaction temperature at 400 rpm for homogeneous mixing with the help of stirrer at pre-set reaction temperature, where the suggested reaction temperature was achieved via heater. When the temperature was achieved, then reaction time was started to count and once reaction time was completed, the heater and stirrer were turned off and the reactor was cooled to room temperature with a cooling coil. Once the room temperature was achieved, the slurry of hydrochar and biochar was removed manually from the reactor vessel and separated with 601-grade Fioroni filter paper. The obtained hydrochar was washed with distilled water to remove any water-soluble

Table 1. Elemental analysis, proximate analysis, and HHV of OPT

Elemental analysis (%)					Proximate analysis (%)				HHV (MJ/kg)
Carbon (%)	Hydrogen (%)	Nitrogen (%)	Sulphur (%)	Oxygen (%)	Moisture (%)	Ash (%)	Volatile matter (%)	Fixed carbon (%)	
40.73	6.05	0.67	0.41	52.14	4.0	1.3	79.3	15.4	13.6

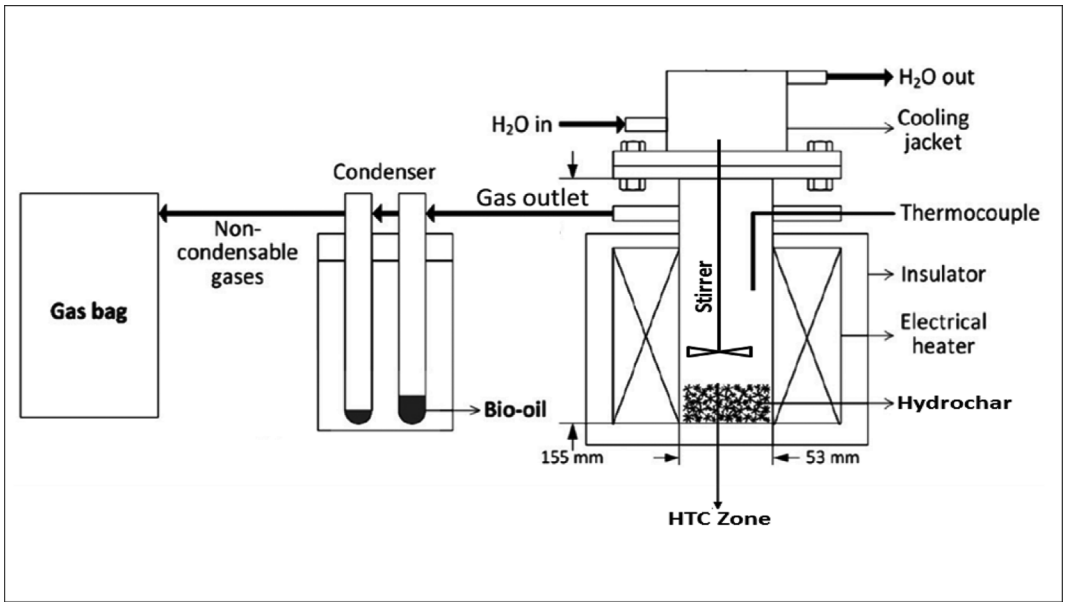

Fig. 3. The experimental reactor used for HTC of OPT.

Table 2. Orthogonal (L9) design matrix showing the effect of process parameters on yield distribution from HTC of OPT

Run#	Temperature (°C)	Reaction time (min)	Particle size (mm)	Solid yield (%)	Liquid yield (%)	Gas yield (%)
R1	180	30	1	42.44	27.94	29.62
R2	180	60	2	39.95	33.30	26.75
R3	180	90	3	41.98	30.91	27.11
R4	200	30	2	30.12	41.26	28.62
R5	200	60	3	28.41	38.61	32.78
R6	200	90	1	30.52	39.17	30.31
R7	220	30	3	27.56	34.26	38.13
R8	220	60	1	24.76	33.30	41.94
R9	220	90	2	21.76	35.86	42.38

products from hydrochar, which was dried at 105 °C for 24 hrs; finally, the materials were weighed, stored in containers to avoid re-moisturization, and characterized for further analysis.

3. Optimization of Solid, Liquid, and Gaseous Yields for HTC of OPT via Taguchi

The Taguchi design method is a simple, systematic, multi-parameter, and vigorous technique for statistical optimization which employs fewer experiments to identify and optimize the effect of process parameters on desired responses [21]. The orthogonal array offers different experiments with different contributions of certain parameters, and the feedback is optimized with respect to signal to noise (S/N) ratio. Hence, the Taguchi method was considered to optimize the parameters of HTC for liquid, gaseous, and solid yields. The different ranges of the optimized parameters were reaction time (30-90 min), particle size (1-3 mm), and reaction temperature (180-220 °C), respectively. The effect of these parameters was optimized for solid yield (%), liquid yield (%), and gas yield (%). A complex design matrix together with respective responses is listed in Table 2.

4. Yield (%) Calculation

The HTC products from this experimental study consisted of solid, liquid, and gas products. For the balance of biomass, the following equations were used to quantify the solid yield ($Y_{hydrochar}$), liquid yield ($Y_{bio\text{-}oil}$) and gas yield (Y_{gas}), respectively, as shown in Eqs, (1), (2) and (3):

$$Y_{hydrochar} = \frac{m_{hydrochar}}{m_{initial}} \times 100 \quad (1)$$

$$Y_{Bio\text{-}oil} = \frac{m_{bio\text{-}oil}}{m_{initial}} \times 100 \quad (2)$$

$$Y_{gas} = 100 - m_{hydrochar} - m_{bio\text{-}oil} \quad (3)$$

where Y indicates the yield percentage and m shows the mass of the sample.

5. Analytical Methods

The existence of functional groups on the sample's surface was determined by FTIR spectrometer analysis (Nicolet iZTM 10 module) between the wavenumber ranging from 4,000 to 400 cm^{-1} on ATIR-FTIR mode. To examine the weight loss and thermal behavior of biomass feedstocks and carbonized samples, thermogravimetry (TGA) was performed by using TGA-Q50, at 800 °C with the

degree of heating by 10 °C/min. The calorific value of solid samples was analyzed by EN 14918 solid biofuels, and of calorific value by utilizing a bomb calorimeter (C2000 model, IKA Werke). Elemental (CHN) analysis was examined according to EN 15104 standard. Furthermore, the quantification of total hydrogen, nitrogen, and carbon content was done through an instrumental method by using a CHN analyzer (Series II CHNS/O Analyzer 2400, Perkin Elmer). The oxygen (O) content was analyzed by difference on a dry basis by following Eq. (4); the energy densification and energy yield (%) were calculated by Eqs. (5) and (6):

$$O\ (\%)=100-(C+H+N+Ad) \quad (4)$$

$$\text{Energy densification}=HHV_{hydrochar}/HHV_{OPT} \quad (5)$$

$$\text{Energy yield}\ (\%)=(m_{hydrochar}/m_{OPT}) * (HHV_{hydrochar}/HHV_{OPT})\times 100 \quad (6)$$

The presence of organic compounds in bio-oil was determined by gas chromatography-mass spectrometry (GC-MS Model: Agilent 7890A) with HP column of HP 5MS (30 m×0.25 mm). The single-phase bio-oil sample was first diluted with acetone by mixing 25 mg of a sample with 1 mL of acetone solution. The temperature of the column oven was adjusted at 35 °C for 2 min and then gradually increased with the heating process of 5 °C/min to 260 °C for 20 min. Helium was used as a carrier gas with a flow rate of 1,000 mL/min. The compounds were identified using the NIST library. The gas mixtures were analyzed and quantified by two gas chromatography equipment with the help of thermal conductivity detectors (Shimadzu GC-8A) with different column packings. Oxygen, hydrogen, nitrogen, and carbon monoxide were analyzed on GC-TCD with a molecular sieve 5A (MS 5A) column. Purified argon gas was used as a carrier gas and temperatures of the column and detector were set at 100 °C. For the analysis of carbon dioxide (CO_2), GC-TCD with Porapak Q column was used and purified helium was used as a carrier gas. The temperatures of the column and detector were set at 80 and 70 °C, respectively. The pure components of each type of anticipated gas were used to plot the calibration curve (volume vs peak area) through which the amount of each gas in the sample was calculated in terms of volumetric percentage.

RESULTS AND DISCUSSION

1. Optimization of Solid, Liquid, and Gaseous Yield via Taguchi Method

It was proposed that hydrothermal processing leads to thermal degradation of feed materials where chemical and physical bonds of feed material get disintegrated, resulting in the formation of simple and small molecules by breaking of large and long-chain compounds such as hemicellulose, cellulose, and lignin. These results were in the dissolution of some molecules to the liquid part, whereas some were degraded to gaseous products and the remainder was obtained as a solid yield [22]. The solid, liquid, and gaseous products were studied as the response for the Taguchi design method, and it was found that the selected range of process parameters showed a significant effect on yield percentages as shown in Table 2. It is evident from Table 2 that the optimized solid yield was accounting for about 42.44% that was obtained at 180 °C, 30 min, and 1 mm, the optimum liquid yield of 41.26% was obtained at 200 °C, 30 min, and 2 mm, whereas the optimized gaseous yield of 42.38% was obtained 220 °C, 90 min and 2 mm. It was also suggested that the higher the difference (the high S/N ratio), the greater will be the effect of the parameter.

It can be observed that low reaction time and low reaction temperature produced high hydrochar yield, whereas the hydrochar yield decreased by increasing reaction temperature and reaction time. The solid yield was higher at low particle size, which decreased by increasing particle size from 1 mm to 2 mm, and again increased by increasing particle size from 2 mm to 3 mm. A reduction in hydrochar yield at higher temperatures is attributed to volatile matter released at higher temperature, which enhanced the dehydration and elimination reactions, hence reducing hydrochar yield [23]. Similarly, a decrease in hydrochar yield with increasing reaction time was due to the reason that higher carbonization times will tend to form permanent gases and light organic compounds as well as longer reaction times support bio-oil formation, consequently reducing the solid yield [24].

It is evident that the particle size, as well as temperature factor, has a correlative effect on the yield of bio-oil, whereas the yield of liquid fuel was decreased at relatively low temperature concerning low particle size, and hence it increased by increasing the reaction temperature to 200 °C with the average particle size to 2 mm, while the yield of liquid fuel started decreasing by gradually increasing the reaction temperature and particle size. On the contrary, the yield of liquid was increasing with increasing the reaction period. Consequently, it is also articulated that during the hydrothermal process the initial biomass was broken and depolymerized into lighter fragments as increasing the reaction temperatures, and then these broken fragments were again reassembled to formulate into new compounds concerning various reactions such as polymerization, condensation, cyclization during the hydrothermal reaction [25]. The trend for liquid yield observed in this study was also supported by previous literature where the effect of temperature was studied on liquid yield produced from barley straw waste and it was also found that the bio-oil yield was increasing at the initial increase in temperatures, whereas the liquid yield started decreasing by the further increase in temperature [26]. Most of the literature suggests a rise in liquid yield up to a specific temperature, whereas increasing temperature beyond that specific temperature results in the reduction of liquid yield [27]. An increase in liquid yield with increasing reaction time from 30 min to 90 min was also supported from previous literature where the effect of reaction time from 30 min to 120 min was investigated and found that the liquid yield was improved by increasing reaction time [28]. Yan et al. [29] and Boocock et al. [30] proposed that longer reaction time is required for higher bio-oil yields.

ANOVA was performed to examine the significance of the process parameters and model. The statistical model is mainly composed of the coefficient of correlation (R2), Fischer's test value (F), and probability values (P) that serve as the basis to relate the significance of the model. Regression analysis is a well-known technique that compares the outcomes of the model with response to statistics [31]. The Fischer's F test forms a relationship between mean squares of the regressed model with residuals (probability due to

Table 3. ANOVA for model 1 (solid yield %)

Source	DF	Adj SS	Adj MS	F-value	P-value
Regression	3	427.246	142.415	17.75	0.004
Temperature	1	421.514	421.514	52.53	0.001
Reaction time	1	5.723	5.723	0.71	0.437
Particle size	1	0.009	0.009	0.00	0.975
Error	5	40.124	8.025	-----	-----
Total	8	467.370	-----	-----	-----

Table 4. ANOVA for model 2 (liquid yield %)

Source	4WDF	Adj SS	Adj MS	F-value	P-value
Regression	3	24.087	8.029	0.34	0.800
Temperature	1	21.169	21.169	0.89	0.389
Reaction time	1	1.025	1.025	0.04	0.844
Particle size	1	1.893	1.893	0.08	0.789
Error	5	119.144	23.829	-----	-----
Total	8	143.231	-----	-----	-----

Table 5. ANOVA for model 3 (gaseous yield %)

Source	DF	Adj SS	Adj MS	F-value	P-value
Regression	3	257.541	85.847	8.89	0.019
Temperature	1	253.110	253.110	26.21	0.004
Reaction time	1	1.961	1.961	0.20	0.671
Particle size	1	2.470	2.470	0.26	0.635
Error	5	48.286	9.657	-----	-----
Total	8	305.827	-----	-----	-----

noise) [32]. The results for these responses were analyzed by ANOVA as shown in Table 3, Table 4, and Table 5 for solid yield, liquid yield, and gaseous yield, respectively.

All linear models were accurately fitted for the designed models for model 1, model 2, and model 3 having the F values of 17.75, 0.34, and 8.89 together with P values of 0.004, 0.800, and 0.019, respectively, that showed the effectiveness of the models. Tables 2 and 3 show the degrees of freedom (DF) representing the experimental data, while Adj SS represents the sum of squares of variation of process factors according to the regression model, whereas Adj MS represents the measurement of adjusted sums of squares of variation of each process factor according to regression models. It was also evident from the ANOVA outcomes (Tables 3, 4, and 5) that F values for process temperature for all the respective models were 26.21 for (gaseous yield), 52.53 (solid yield), and 0.89 (liquid yield), respectively, representing that the process temperature was one of the most significant factors for all the presented models. Consequently, the regression model equations for models 1, 2, and 3 are given in Eqs. (7), (8), and (9), respectively.

$$\textbf{Solid yield} = 117.6 - 0.4191\ \text{temperature} - 0.0326\ \text{reaction time} + 0.04\ \text{particle size} \quad (7)$$

$$\textbf{Liquid yield} = 14.2 + 0.0939\ \text{temperature} + 0.0138\ \text{reaction time} + 0.56\ \text{particle size} \quad (8)$$

$$\textbf{Gaseous yield} = -31.7 + 0.3248\ \text{temperature} + 0.0191\ \text{reaction time} - 0.64\ \text{particle size} \quad (9)$$

2. Characterization of Hydrochar

2-1. Elemental Analysis, H/C and O/C Atomic Ratios, HHV and Energy Densification

Elemental (CHNS/O) analysis is considered important because it tends to determine the quantity and composition of gases removed during combustion together with the amount of gases needed to burn the biomass, biofuel, or fuel [33]. Therefore, CHNS/O analysis was conducted for hydrochars produced from all nine runs, and these results were reported in Table 6. Generally, more carbon and less oxygen was desirable because less oxygen and high carbon content lead to higher HHV values, subsequently improving the energy and combustion properties. Based on overall findings and results, it can be claimed that the HTC process resulted in the enrichment of carbon and reduction of oxygen in hydrochar samples, subsequently enhancing the energy and combustion characteristics. Higher carbon content and lower oxygen content of hydrochars confirmed that HTC has transformed low energy OPT into high energy solid fuel (hydrochar). As shown in Table 1, the OPT consisted of 40.7% carbon, 6.1% hydrogen, 0.7% nitrogen, 0.4% sulfur, and 52.1% oxygen, respectively (by difference) [33]. On the other hand, the CHNS/O values for hydrochars ranged 57.1-68.8% carbon, 0.14-2.39% hydrogen, 1.11-1.67% nitrogen, and

Table 6. Elemental (CHNS/O) analysis, H/C and O/C atomic ratios, HHV, and energy densification of hydrochars produced from HTC of OPT

	Elemental analysis (%)					H/C	O/C	HHV (MJ/kg)	Energy densification ratio	Energy yield (%)
	C	H	N	S	O					
R1	66.36	1.18	1.53	0.37	30.56	0.02	0.46	21.8	1.28	54.32
R2	68.83	0.32	1.51	0.33	29.01	0.01	0.42	20.4	1.32	52.73
R3	64.42	0.22	1.67	0.41	33.28	0.01	0.52	20.5	1.31	54.99
R4	57.10	0.43	1.49	0.45	40.53	0.02	0.71	21.2	1.36	40.96
R5	66.55	2.39	1.04	0.39	29.63	0.04	0.45	20.8	1.33	37.79
R6	63.94	0.41	1.11	0.34	34.20	0.01	0.53	20.9	1.34	40.90
R7	62.52	0.32	1.16	0.28	32.72	0.01	0.51	19.9	1.40	38.58
R8	58.76	0.14	1.62	0.30	39.18	0.01	0.67	20.8	1.33	32.93
R9	64.27	0.58	1.71	0.38	33.06	0.01	0.51	21.4	1.37	29.81

29.01-40.53% oxygen, respectively, as shown in Table 6.

The removal of oxygen and enrichment of carbon in hydrochars after the HTC process led to higher HHVs, which may be attributed to the reaction parameters (reaction temperature and reaction time), humidity as well as to deoxygenation reactions, taking place during the HTC process. It is recommended that the reaction temperature and humidity have the opposite effect on carbon content, ultimately on HHV. For instance, high reaction temperature and low humidity will result in an increased carbon content, subsequently increasing the HHV. On the other hand, low reaction temperature and high humidity will decrease carbon content and consequently low HHV [32].

It is recommended that HHV of bio-oil commonly falls in the range of 16-19 MJ/kg [34]. Gómez et al. [35] studied the effect of reaction temperature on HHV of bio-oils and found that there was not a significant effect of increasing temperature on HHV of bio-oil. It was found that the bio-oil produced at low temperature had greater HHV value than that produced at high temperature. This might be attributed to the higher HHV of individual condensable vapors, which was promoted by supportive cracking reactions. Another study also reported similar findings suggesting that the HHV of bio-oil was not altered by increasing reaction temperature [36].

The improvement in CHNS/O analysis can further be investigated and correlated to the fuel quality by H/C and O/C atomic ratio as shown in Table 6. Generally, the fuels with low H/C and O/C atomic ratio values are considered better fuels, because the low H/C and O/C atomic ratio fuels will generate fewer water vapors and less smoke during combustion with the minimum energy loss [37]. Based on results, it can be confirmed that the H/C and O/C atomic ratio values of raw OPT were 0.15 and 1.28, respectively, whereas the H/C and O/C atomic ratios of hydrochars ranged between 0.01-0.2 H/C and 0.42-0.71 O/C, which was lower than those of rice husk. A decrease in O/C and H/C atomic ratio values may be related to exothermic oxidation of hydrogen and carbon to H_2O, CO, and CO_2 during the HTC process [38]. It is reported in the previous literature that the decreased values of H/C and O/C atomic ratios confirm that the aromaticity was strengthened gradually [39] due to higher temperature, time, demethylation, dehydration, and decarboxylation reactions [40]. It is also confirmed that partially carbonized products with lower O/C and H/C atomic ratios are formed during the carbonization process [41].

The energy densification represents the effectiveness of any process where high energy density values show greater effectiveness of the process. It has been reported that during HTC, reaction parameters of HTC, dehydration, decarboxylation, condensation reactions, and higher carbonization improve energy densification [33]. It is recommended that energy density values greater than 1 represent higher efficiency of the process. As shown in Table 6, the energy densification value of hydrochars was between 1.28 and 1.40, which confirmed the significance of the HTC process. An improvement in energy densification values of hydrochars has been reported previously in the literature [40]. HHV is one of the most important energy properties of fuels, biofuels, and biomass materials, which tends to determine the amount of energy available in materials [40]. Therefore, the HHV of hydrochars was assessed to find the suitability of hydrochars as a solid fuel. The HHV of OPT was 13.6 MJ/kg (Table 1), which was increased to 19.9-21.8 MJ/kg for hydrochars (Table 6). This enhancement in HHV values can be related to the reaction temperature of the process. The higher reaction results in greater carbon content, subsequently higher values of HHV [42]. Further, an increase in HHV values may be correlated to the reaction time; it is stated in the literature that the HHV increases by increasing the reaction time of the carbonization process, which represent the level of carbonization achieved during carbonization [40].

2-2. FTIR Analysis of OPT and Hydrochar

The analysis of FTIR spectra revealed the respective wavenumber ranging from 4,000 to 400 cm^{-1} was attempted to analyze the configuration of functional groups of OPT, as well as hydrochar produced by the HTC process. The analysis of these compounds' spectra governs the information of the presence of various bonds and visualized the molecular structure of these analyzed compounds [43]. The analysis of these observed emission spectra administrated the existence of different bonding patterns and envisioned the molecular mechanisms of these analyzed compounds. The data achieved for the solid product analyzed by spectral analysis and OPT by FTIR is shown in Fig. 4. The obtained absorbance peaks for hydrochar were relatively found to be the same as that for OPT. The peaks containing -OH groups were observed at 3,417-3,430 cm^{-1}, which happened due to the overlapping of the N-H bonding patterns of amino groups [44], whereas due to the high reaction temperatures, a decrease in O-H bond was observed, which pointed out that the OPT material was dehydrated and the water in solids was removed. Furthermore, similar peaks trends were also achieved at 2,923 cm^{-1} and 2,853 cm^{-1} due to the vibrational movement between C-H bonds. These observed peaks were to be lower in hydrochar when compared with OPT. Therefore, it was elaborated that during the HTC process the hydrogen had been discharged from the reaction. The observed peak found at 1,457 cm^{-1} belongs to the CH_2 bond. While some other peaks were also at 1,608 cm^{-1}, 1,613 cm^{-1}, 1,513 cm^{-1} peaks due to the vibrational stretching between C-C and C=C bonds. The bond found at 1,273 cm^{-1} showed the presence of carboxylic acid content. The peak around 1,113 cm^{-1} and 1,165 cm^{-1} was because of C-O-C stretch-

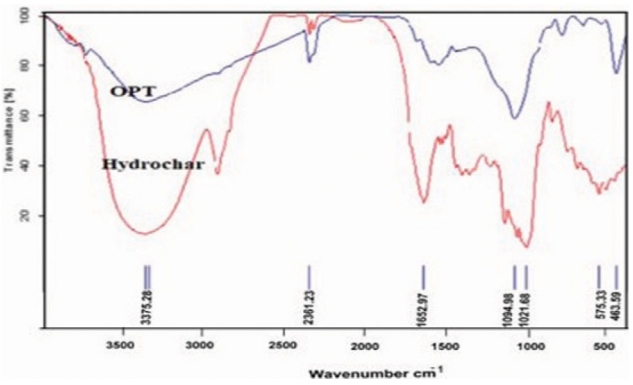

Fig. 4. FTIR analysis of OPT and hydrochar produced at optimized conditions (R1) (180 °C, 30 min, and 1 mm).

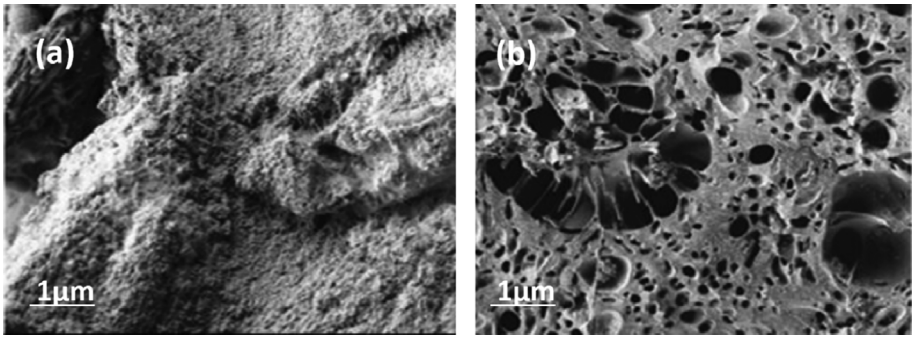

Fig. 5. SEM analysis of (a) OPT and (b) hydrochar produced at optimized conditions (R1) (180 °C, 30 min, and 1 mm).

ing vibration.

2-3. SEM Analysis of OPT and Hydrochar

Scanning electron microscopy (SEM) is used to analyze the structural and geometrical properties of biomass and its products produced by different methods. The SEM images of the OPT and optimized hydrochar are given in Fig. 5(a) and (b), respectively. The predicted morphological geometry of the hydrochar was observed due to the pores' formation on its surface, which significantly anticipated that the structural transformation of the OPT appeared during the HTC process. The obtained result revealed that the lignocellulosic structure of the OPT was destroyed during the HTC process. Furthermore, it is evident from Fig. 5(a) that there were no pores on the surface of OPT; in contrast, the formation of the pores on hydrochar surface (Fig. 5(b)) was monitored due to the removal of some volatile matter on the surface of hydrochar during the HTC process [45]. The formation of pores on the surfaces of hydrochar was sustainably triggered by the reaction time and reaction temperature of HTC, where the cellulose and hemicellulose were decomposed at higher reaction times significantly, resulting in the formation of pores on the hydrochar surface [46]. It is reported that at higher temperatures, the biomass was significantly degraded because of the exposure of biomass layers due to the increasing temperatures improved the porosity of the hydrochar surface. Marx et al. [47] reported that at higher temperature, the walls of the closer pores were affected and destroyed, which resulted in increasing the pore size diameter. The structural configuration on the surface of hydrochar thus showed the dewatering of the hydrochar more readily during the filtration process because the hydrochar pores allowed the water drainage from the products of the HTC process. The porous structure of hydrochar is suitable to utilize for sequestration and adsorption applications [48]. Though the porosity of hydrochar was enhanced after HTC and was observed to be higher than OPT, however, it still needs to be improved; therefore, it is comprehensively demonstrated from the previous literature that the porosity of hydrochars seemed to be low because of the deposition of secondary microspheres on the top end of the primary chars. Therefore, it is recommended that the activation of hydrochars either by (chemical or physical) methods is vital to achieve a higher degree of porosity, thus enhancing the adsorption of hydrochar capacity.

2-4. TGA Analysis of OPT and Hydrochar

TGA is considered as one of the most useful tools to measure

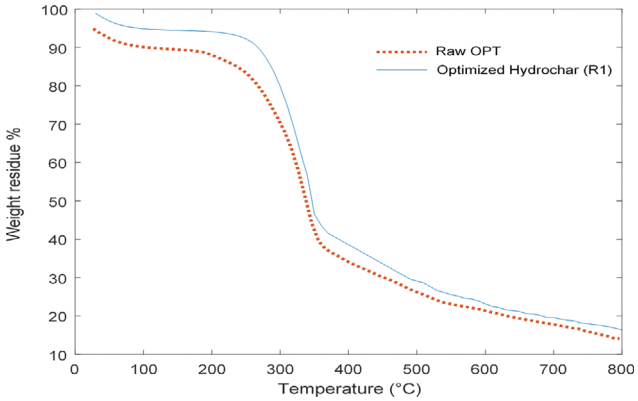

Fig. 6. TGA analysis of OPT and hydrochar.

the thermal stability and weight loss behavior of samples at different temperatures and times under a controlled environment. Therefore, the thermal stability and weight loss behavior of OPT and hydrochar was assessed by using TGA, and result is shown in Fig. 6. It is evident from Fig. 6 that the initial surface moisture was removed up to 150 °C, after that there was a significant weight loss 370 °C, which was ascribed to the decomposition of hemicellulose and cellulose components resulting in the formation of gases and low volatiles [32]. There was a decrease in weight loss after this temperature, which may be attributed to presence of lignin content. On the other hand, it can be noted from Fig. 6 that the OPT was less thermally stable than hydrochar, suggesting that the HTC transformed less thermally stable material, i.e., OPT to high thermally stable material, i.e., hydrochar. It can be confirmed that the OPT experienced rapid weight loss, consequently was less thermally stable, which suggests that incomplete combustion occurred, resulting in high emission of pollutants. An improvement in thermal stability of hydrochar may be correlated to the reaction temperature of HTC [1].

3. GCMS Analysis of Bio-oil

The major components found in liquid products (bio-oil) by GC-MS are compared in Fig. 7(a) and the representative example of the GC-MS graph is presented in Fig. 7(b). In the bio-oils, there were respective 13 major organic compounds that had been detected and analyzed, having a probability greater than 90% against the NIST library. The most significant organic material in the bio-oil

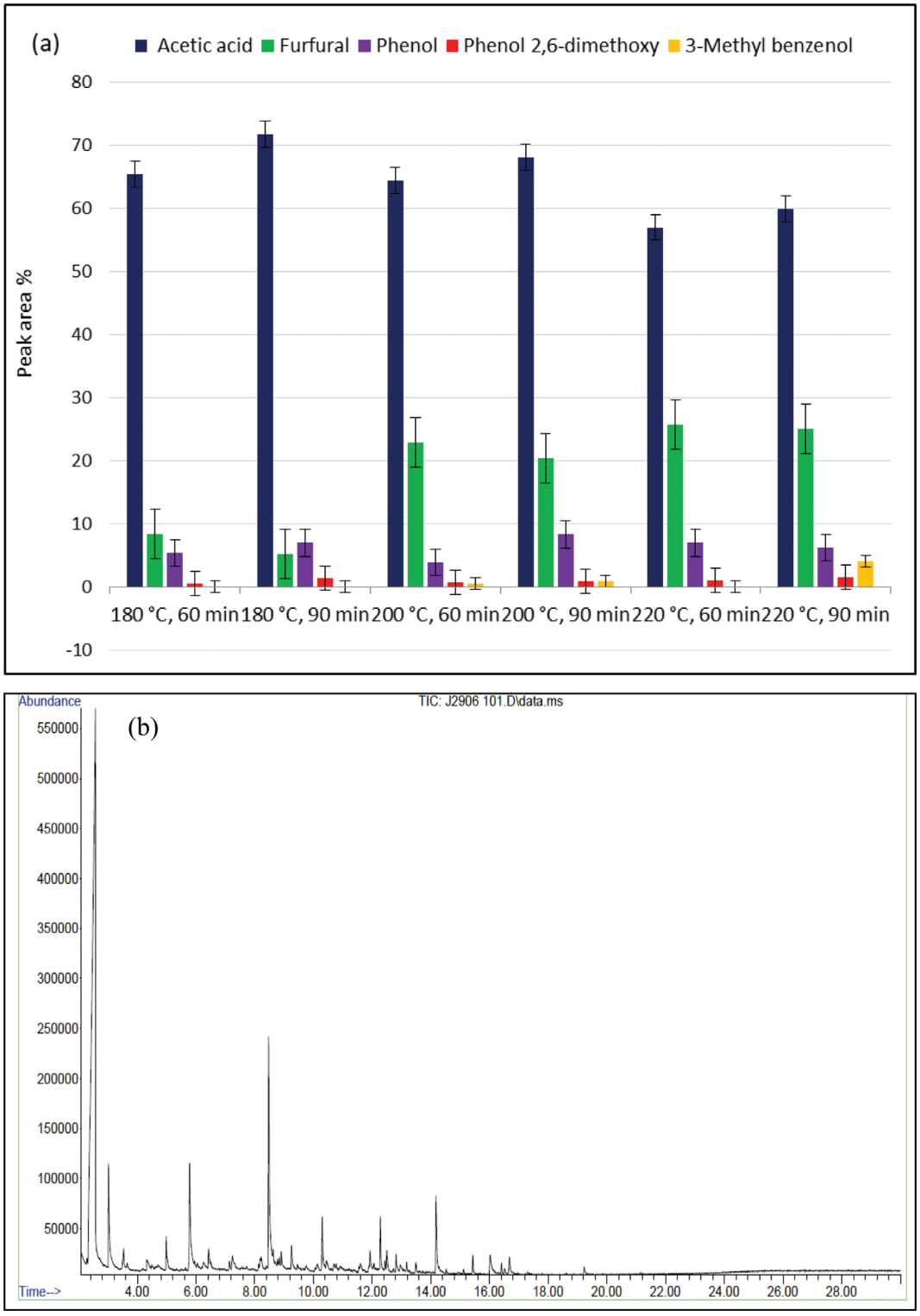

Fig. 7. (a) Major organic components in bio-oil produced from the HTC of OPT and (b) chromatogram of bio-oil obtained from GC-MS at optimized conditions for bio-oil yield (R4) 200 °C, 30 min, and 2 mm.

detected by GC-MS analysis was acetic acid, followed by phenol and furfural, respectively. From the previous literature, these are the major organic factors present in bio-oil produced from the HTC process [49,50]. Along with these components, other organic compounds were detected which include phenol 2,6-dimethoxy, 3-methyl benzenol, propanoic acid, etc.

The presence of acetic acid in bio-oil was attributed to the decomposition of acetoxy-group attached to xylose in hemicellulose

Table 7. Outlet gas compositions (volume %)

Gaseous composition	R1	R2	R3	R4	R5	R6	R7	R8	R9
H_2	0.31	0.79	1.09	1.41	1.58	1.71	1.78	1.85	1.97
CO	1.92	4.94	5.84	1.07	5.13	7.15	1.98	7.89	7.19
CO_2	3.88	9.18	17.91	6.18	17.07	20.81	10.18	25.66	29.02
CH_4	0.87	1.32	2.85	1.92	2.85	4.28	3.92	5.92	9.17

of the biomass [51], and the decomposition of lignin results in the formation of phenol and other phenolic compounds [52]. The formation of acids, alcohols, phenols, and furfurals might be attributed to the thermal degradation of cellulosic and hemicellulose components of OPT during the HTC [53]. The acid formation in bio-oils can be attributed to the decomposition of extractives present in biomass [54]. It is also reported by previous literature that the carboxylic acids are prepared through hydrolysis/dehydration of lignocellulosic materials or by the wood extracts.

4. GC-TCD of Gaseous Composition

The gaseous products released during the HTC of OPT contained a mixture of CO_2, CO, H_2, and a small amount of CH_4 as shown in Table 7. Each gas was proportional to the reaction time and HTC temperature. At certain levels, the decomposition level for complex reactions and OPT together with the formed gases and biomass produced during the HTC process. At high temperatures, decarboxylation of acetyl groups from herbaceous biomass accelerated and this caused an increase in CO_2 formation. According to Chen et al. [55], decarboxylation and depolymerization of lignocellulosic components are the primary reactions during thermal degradation irrespective of biomass type and atmospheric condition. The controlling factor in the primary reaction of biomass that leads to the formation of CO_2 is influenced by the temperature, which causes depolymerization of covalent bonds of lignocellulosic materials. The formation of CO during HTC is due to the de-carbonylation of hemicellulose and cellulose [56]. Because of this, an increment in HTC temperature accelerates the de-carbonylation reaction in biomass.

CONCLUSIONS

This study optimized the effect of process parameters of HTC for hydrochar, bio-oil and gaseous yields through the Taguchi method. It was found that higher temperature yielded more biogas, intermediate temperature produced higher bio-oil yield, whereas lower temperature favored hydrochar yield, which confirms the significance of reaction temperature on yield distribution during HTC of OPT. As anticipated, depolymerization and decarboxylation were the primary reactions occurring during HTC of OPT, which caused thermal degradation of the lignocellulosic structure of biomass at intermediate and higher temperatures, hence producing more bio-oil and biogas, respectively. Furthermore, the carbon content and HHV were increased, whereas oxygen, O/C, and H/C atomic ratios were decreased for hydrochar as compared to OPT, suggesting that hydrochar can serve as a better fuel than OPT itself. The major component in bio-oil composition was acetic acid followed by furfural, phenol, phenol 2,6-dimethoxy, and creosol while the gaseous product was composed of CH_4, CO_2, CO, and H_2.

Based on the overall findings of this study, it can be recommended that the OPT hydrochar has potential application as a solid fuel, carbon material, energy, and agricultural applications. Furthermore, future studies in this research area can elaborate on the effect of other process parameters, that can assess the effect of conventional and microwave heating systems as well as the various applications of hydrochars produced from HTC of OPT.

CONFLICT OF INTEREST

The authors declare no conflict of interest.

REFERENCES

1. S. Nizamuddin, N. S. Jayakumar, J. N. Sahu, P. Ganesan, A. W. Bhutto and N. M. Mubarak, *Korean J. Chem. Eng.*, **32**, 1789 (2015).
2. L. Fan, P. Sun, L. Yang, Z. Xu and J. Han, *Korean J. Chem. Eng.*, **37**(1), 166 (2020).
3. S. Kim, Y. F. Tsang, E. E. Kwon, K. Y. A. Lin and J. Lee, *Korean J. Chem. Eng.*, **36**(1), 1 (2019).
4. H. N. Tran, S. J. You and H. P. Chao, *Korean J. Chem. Eng.*, **34**(6), 1708 (2017).
5. Y. Li, N. Song and K. Wang, *Korean J. Chem. Eng.*, **36**(5), 678 (2019).
6. A. Brown, B. McKeogh, G. Tompsett, R. Lewis, N. Deskins and M. Timko, *Carbon*, **125**, 614 (2017).
7. K. Sun, J. Tang, Y. Gong and H. Zhang, *Environ. Sci. Pol. Res.*, **22**, 16640 (2015).
8. L.-P. Xiao, Z.-J. Shi, F. Xu and R.-C. Sun, *Bioresour. Technol.*, **118**, 619 (2012).
9. S. Nizamuddin, H. A. Baloch, G. J. Griffin, N. M. Mubarak, A. W. Bhutto, R. Abro, S. A. Mazari and B. S. Ali, *Renew. Sustain. Energy Rev.*, **73**, 1289 (2017).
10. S.-H. Kong, S.-K., Loh, R. T. Bachmann, S. A. Rahim and J. Salimon, *Renew. Sustain. Energy Rev.*, **39**, 729 (2014).
11. W. Ismail, T. M. Thaim and R. A. Rasid, *Biomass. Bioenergy*, **124**, 83 (2019).
12. F. Abnisa, A. Arami-Niya, W. W. Daud, J. Sahu and I. Noor, *Energy Convers. Manage.*, **76**, 1073 (2013).
13. Y.-L. Loow and T. Y. Wu, *J. Environ. Manage.*, **216**, 192 (2018).
14. K. H. D. Tang and H. M. Al Qahtani, *Environ. Develop. Sustain.*, **22**, 4999 (2020).
15. S. Nizamuddin, S. S. Qureshi, H. A. Baloch, M. T. H. Siddiqui, P. Takkalkar, N. M. Mubarak, D. K. Dumbre, G. J. Griffin, S. Madapusi and A. Tanksale, *Materials*, **12**, 403 (2019).
16. J. Fang, L. Zhan, Y. S. Ok and B. J. Gao, *J. Ind. Eng. Chem.*, **57**, 15 (2018).

17. S. Kumar, V. A. Loganathan, R. B. Gupta and M. O. Barnett, *J. Environ. Manage.*, **92**, 2504 (2011).
18. Y. Xue, B. Gao, Y. Yao, M. Inyang, M. Zhang, A. R. Zimmerman and K. S. Ro, *Chem. Eng. J.*, **200**, 673 (2012).
19. L. Dai, B. Wu, F. Tan, M. He, W. Wang, H, Qin, X. Tang, Q. Zhu, K. Pan and Q. Hu, *Bioresour. Technol.*, **161**, 327 (2014).
20. H. H. Hammud, A. Shmait and N. Hourani, *RSC Adv.*, **5**, 7909 (2015).
21. H. A. Baloch, M. Siddiqui, S. Nizamuddin, N. Mubarak, M. Khalid, M. Srinivasan and G. Griffin, *Proc. Safety Environ. Prot.*, **137**, 300 (2020).
22. A. T. Yuliansyah, T. Hirajima, S. Kumagai and K. Sasaki, *Waste. Biomass. Valor.*, **1**, 395 (2010).
23. B. B. Uzun, E. Apaydin-Varol, F. Ateş, N. Özbay and A. E. Pütün, *Fuel*, **89**, 176 (2010).
24. A. Arami-Niya, F. Abnisa, M. S. Sahfeeyan, W. W. Daud and J. N. Sahu, *BioResources*, **7**, 0246 (2012).
25. H. Huang, X. Yuan, G. Zeng, J. Wang, H. Li, C. Zhou, X. Pei, Q. You and L. Chen, *Fuel Process. Technol.*, **92**, 147 (2011).
26. Z. Zhu, L. Rosendahl, S. S. Toor, D. Yu and G. Chen, *Appl. Energy*, **137**, 183 (2015).
27. H. A. Baloch, S. Nizamuddin, M. Siddiqui, S. Riaz, A. S. Jatoi, D. K. Dumbre, N. Mubarak, M. Srinivasan and G. Griffin, *J. Environ. Chem. Eng.*, **6**, 5101 (2018).
28. K. Anastasakis and A. Ross, *Bioresour. Technol.*, **102**, 4876 (2011).
29. Y. Yan, J. Xu, T. Li and Z. Ren, *Fuel Process. Technol.*, **60**, 135 (1999).
30. D. Boocock and K. Sherman, *Can. J. Chem. Eng.*, **63**, 627 (1985).
31. K. Intani, S. Latif, A. R. Kabir and J. Müller, *Bioresour. Technol.*, **218**, 541 (2016).
32. M. Siddiqui, S. Nizamuddin, N. Mubarak, K. Shirin, M. Aijaz, M. Hussain and H. A. Baloch, *Waste. Biomass. Valor.*, **10**, 521 (2019).
33. S. Nizamuddin, M. T. H. Siddiqui, H. A. Baloch, N. M. Mubarak, G. Griffin, S. Madapusi and A. Tanksale, *Environ. Sci. Pol. Res.*, **25**, 17529 (2018).
34. Q. Zhang, J. Chang, T. Wang and Y. Xu, *Energy Convers. Manage.*, **48**, 87 (2007).
35. N. Gómez, S. Banks, D. Nowakowski, J. Rosas, J. Cara, M. Sánchez and A. Bridgwater, *Fuel Process. Technol.*, **172**, 97 (2018).
36. S. Thangalazhy-Gopakumar, S. Adhikari, H. Ravindran, R. B. Gupta, Q. Fasina, M. Tu and S. D. Fernando, *Bioresour. Technol.*, **101**, 8389 (2010).
37. Z. Liu, A. Quek, S. K. Hoekman and R. Balasubramanian, *Fuel*, **103**, 943 (2013).
38. G. K. Parshetti, S. Chowdhury and R. Balasubramanian, *Biresour. Technol.*, **161**, 310 (2014).
39. H. Lin, S. Wang, L. Zhang, B. Ru, J. Zhou and Z. Luo, *Chin. J. Chem. Eng.*, **25**, 232 (2017).
40. S. E. Elaigwu and G. M. Greenway, *J. Anal. Appl. Pyrol.*, **118**, 1 (2016).
41. M. Guiotoku, C. Rambo, F. Hansel, W. Magalhaes and D. Hotza, *Mater. Lett.*, **63**, 2707 (2009).
42. P. Zhao, Y. Shen, S. Ge and K. Yoshikawa, *Energy Convers. Manage.*, **78**, 815 (2014).
43. D. T. Chadwick, K. P. McDonnell, L. P. Brennan, C. C. Fagan and C. D. Everard, *Renew. Sustain. Energy Rev.*, **30**, 672 (2014).
44. J. Park, S. W. Won, J. Mao, I. S. Kwak and Y.-S. Yun, *J. Hazard. Mater.*, **181**, 794 (2010).
45. O. O. Afolabi, M. Sohail and C. Thomas, *Waste. Biomass. Valor.*, **6**, 147 (2015).
46. Y. Gao, X. Wang, J. Wang, X. Li, J. Cheng, H. Yang and H. Chen, *Energy*, **58**, 376 (2013).
47. S. Marx, I. Chiyanzu and N. Piyo, *Bioresour. Technol.*, **164**, 177 (2014).
48. S. Kannan, Y. Gariepy and G. V. Raghavan, *Energy Fuel*, **31**, 4068 (2017).
49. J. S. Tumuluru, S. Sokhansanj, C. T. Wright and T. Kremer, *Adv. Gas Chromatogr. Agric. Biomed. Indistrial Appl.*, 211 (2012).
50. Y. Uemura, V. Sellappah, T. H. Trinh, S. Hassan and K.-i. Tanoue, *Bioresour. Technol.*, **243**, 107 (2017).
51. M. J. Prins, K. J. Ptasinski and F. J. Janssen, *J. Anal. Appl. Pyrol.*, **77**, 35 (2006).
52. C. A. Mullen, A. A. Boateng, N. M. Goldberg, I. M. Lima, D. A. Laird and K. B. Hicks, *Biomass. Bioenergy*, **34**, 67 (2010).
53. G. W. Huber, S. Iborra and A. Corma, *Chem. Rev.*, **106**, 4044 (2006).
54. M. K. Jindal and M. K. Jha, *RSC Adv.*, **6**, 41772 (2016).
55. D. Chen, A. Gao, K. Cen, J. Zhang, X. Cao and Z. Ma, *Energy Convers. Manage.*, **169**, 228 (2018).
56. T. Bridgeman, J. Jones, I. Shield and P. Williams, *Fuel*, **87**, 844 (2008).